e-ISSN: 2550-164X

Available online at
https://jmeche.uitm.edu.my/

Journal of Mechanical Engineering 23(1) 2026, 132 – 144.

Journal of Mechanical Engineering

Influence of Heat Input on Mechanical and Microstructure Features of AISI 304 Austenitic Stainless-steel Joints Fabricated by TIG Spot Welding

Mohammed K. Aljanabi[1], Marwah Mohammed Abdulridha[1], Ekhlas Hassan[1], Zainab Al-Khafaji[2, 3,*]

[1]*Department of Materials Engineering, Faculty of Engineering, University of Kufa, Najaf, Iraq*
[2]*Department of Civil Engineering, Faculty of Engineering and Built Environment, Universiti Kebangsaan Malaysia, 43600 UKM Bangi, Selangor, Malaysia*
[3]*Imam Ja'afar Al-Sadiq University, Qahira, Baghdad, Iraq*

ARTICLE INFO

Article history:
Received 09 August 2025
Revised 03 November 2025
Accepted 20 November 2025
Online first
Published 15 January 2026

Keywords:
Resistance spot welding (RSW)
AISI 304 austenitic stainless steel
Gas tungsten arc welding (GTAW)
Spot welding

DOI:
10.24191/jmeche.v23i1.8443

ABSTRACT

The welding experiments were performed with a current range of 45 A to 90 A, a welding time of 3 s to 5 s, and an electrode-to-cup gap of 1.5 mm to 3.0 mm under pure argon shielding gas. Based on process parameters, the heat input domain was associated with nugget diameter, ambient ferrite morphology, tensile shear strength of weld joints, and the nature of fracture and the microhardness distribution in fusion zone (FZ), partially melted zone (PMZ), and heat-affected zone (HAZ). Examinations by optical and scanning electron microscopy showed that all weld zones comprised δ-ferrite in an austenitic matrix, whose morphology evolved from lath to vermicular scales with increasing heat input. Maximum tensile shear strength (4179 N) and weld toughness (5.529 J) were achieved for a balanced δ-ferrite content and an optimal average nugget size of 5.65 mm at 75 A, 3 s, and 1.5 mm, over high heat input of 90 A produced low mechanical features by over penetration and grain coarsening. The microhardness of the welded region increased to about 250 HV at a medium heat input. In contrast, a high heat input resulted in coarsening of δ-ferrite and a decrease in hardness. All fractures initiated in the PMZ, which was determined to be a critical region for joint failure. These results provide a process–structure–property framework to guide the optimization of tungsten inert gas (TIG) spot-welding parameters for thin-gauge stainless steels requiring high joint integrity.

[2*] Corresponding author. *E-mail address*: p123005@siswa.ukm.edu.my
https://doi.org/10.24191/jmeche.v23i1.8443

INTRODUCTION

With the best in-process efficiency, the lowest joint dilution, no consumables required, and significant weight reduction, resistance spot welding (RSW) still stands as the most common spot joining method for automotive sheets (Aliyari et al., 2025). In several of these uses, there is little or no access to both sheet sides for the RSW process (Groover, 2012). Consequently, a new joining method must be developed for thin sheets, providing the necessary strength with access from only one side. In this regard, tungsten inert gas (TIG) welding could be a solution, as it allows one-sided joining while controlling the heat input to ensure sufficient strength (Cai et al., 2023). Among the electric arc welding processes, gas tungsten arc welding (GTAW) is unique in that the welding arc is based on a non-consumable tungsten electrode. The inert gas used to protect the weld makes it perceived as one of the most efficient processes for producing high-quality welds.

Furthermore, in some applications, it enables welding without using filler material; this type of welding is referred to as autogenous welding (Singh & Agrawal, 2021). In the GTAW process, various factors, such as voltage, heat input, and current time, play an important role in the final properties of the material (Muñoz et al., 2021). This technique can work with direct (DC) and alternating current (AC). The current pulse width may be varied to accommodate different material thicknesses, and there is a defined current setting for each material type. An AC TIG welding machine outputs alternating positive and negative polarity currents that apply to the weld of either steel or aluminum and their alloys (Casanueva et al., 2023; Muñoz et al., 2021). Stainless steel is indeed a significant metal alloy comprising iron, to which given additions were made, including Carbon (C), Aluminum (Al), Silicon (Si), Molybdenum (Mo), Nickel (Ni), and Chromium (Cr) (Pasupulla et al., 2022; Radhi et al., 2023; Radhi & Al-Khafaji, 2018). 304 stainless steel, a standard austenitic stainless steel, is widely used in the chemical processing, aerospace, and transportation industries due to its good corrosion resistance and mechanical properties (Chen et al., 2024). Although there have been numerous reports on the GTAW of stainless steels, most research has focused on bead-on-plate and continuous seam welds rather than on TIG spot welding thin-gage austenitic stainless steels such as AISI 304. This is important for TIG spot welding, which is highly affected by thermal conditions, localized heat input, and rapid solidification during the weld process (Casanueva et al., 2023; Kumar & Shahi, 2011). The application of GTAW techniques to join dissimilar steels has been the subject of several studies. Hayat and Aminy, (2022) observed that as the welding current increases, the nugget diameter increases, thereby improving the joints' load-bearing capacity.

Furthermore, the TIG-spot welding approach might be used to generate a suitable pull-out mode of failure with totally ductile fracture (Rajak et al., 2023). The impact of welding parameters on the nugget diameter of 1 mm DP590 steel sheets was examined by Banerjee et al. (2016). They found that the nugget diameter increased in the favorable weldability range before expulsion when the welding current and time were increased. Similarly, Kishore et al. investigated how various welding conditions affected the nugget size and load-bearing capacity of RSW joints made from 1.3 mm thick galvanized and bare DP600 steel sheets under tensile-shear and coach-peel conditions (Kishore et al., 2019). Sabzi et al. (2021) demonstrated that the hardness and fracture energy of weld metal (WM) increased significantly with changes in welding parameters. In particular, while previous studies have established that heat input critically governs δ-ferrite formation, where lower heat inputs promote finer lathy morphologies and higher mechanical features. Excessive heat promotes vermicular or skeletal ferrite, associated with reduced toughness (Tabrizi et al., 2021). These microstructural–mechanical relationships have rarely been quantified under TIG spot-welding conditions. Furthermore, although optimal δ-ferrite fractions (5% – 10%) have been reported to enhance ductility, toughness, and resistance to solidification cracking in austenitic stainless steels (Arh et al., 2021; Chuaiphan & Srijaroenpramong, 2020), no comprehensive studies have systematically correlated welding current, time, and electrode-to-cup distance with δ-ferrite morphology, nugget geometry, and mechanical performance in spot-welded 304 stainless steel. This lack of process–structure property mapping limits the

https://doi.org/10.24191/jmeche.v23i1.8443

industry's ability to define robust welding windows for high-integrity one-sided joints, particularly in applications where thin-gauge stainless steel is used in critical service environments.

The present study addresses a critical gap in welding metallurgy by providing a systematic process–structure–property analysis of TIG spot welding of thin-gauge AISI 304 austenitic stainless steel, a joining method of increasing industrial relevance in applications where access to one side of the joint is restricted. While prior investigations have examined the influence of heat input on δ-ferrite formation in continuous GTAW processes, there is a paucity of research quantifying the morphological transitions of δ-ferrite (lathy, vermicular, globular) under the rapid thermal cycles inherent to spot welding, and correlating these changes with nugget geometry, mechanical strength, and fracture location. This study is novel in its integrated approach, simultaneously varying welding current, dwell time, and electrode-to-gas cup distance to generate a controlled range of heat inputs, while employing optical and scanning electron microscopy alongside mechanical and microhardness testing to establish direct quantitative links between process parameters, δ-ferrite morphology, and weld performance. The aim is to identify an optimal welding window that maximizes tensile shear strength, weld toughness, and hardness while mitigating over-penetration and microstructural coarsening. The outcomes provide not only fundamental insights into heat input–microstructure interactions in TIG spot welds but also practical guidance for industry in fabricating high-integrity one-sided joints for thin stainless-steel components in sectors such as transportation, food processing, and chemical equipment manufacturing.

EXPERIMENTAL/ THEORETICAL DETAILS

Materials

In this study, AISI 304 stainless steel sheets are used. As shown in Fig 1, the sheets have dimensions of 100 × 25 × 1 mm. Table 1 demonstrates the chemical analysis of the 304 stainless steel examined in this research.

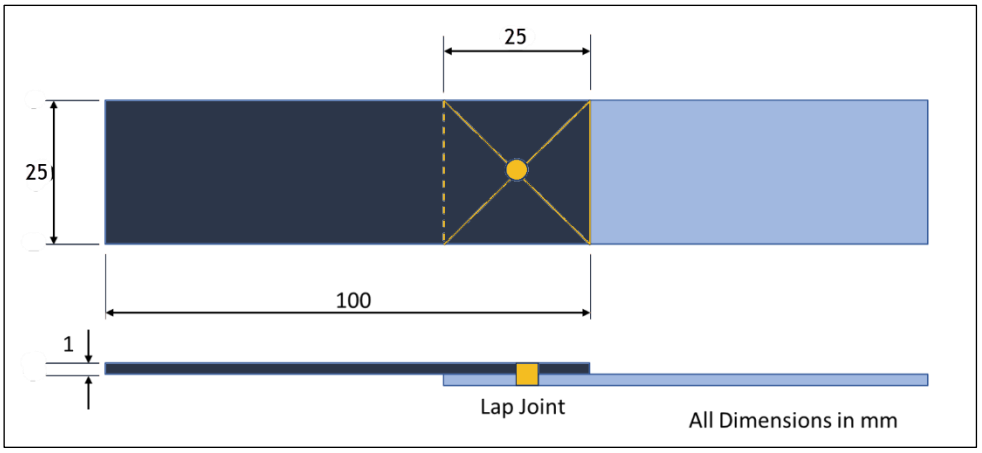

Fig. 1. The weld joints' dimensions.

Table 1. AISI 304 stainless steel chemical analysis

Element wt %	C	Si	Mn	Cr	Ni	Fe
Obtained	0.03	0.52	1.3	18.1	8	Bal.

https://doi.org/10.24191/jmeche.v23i1.8443

TIG - spot welding procedure

TIG machine (Miller-The diversion 165 model) was used in the research. Joints were designed to be fixed on a table, as shown in Fig 2(a). The Welding parameters of TIG used are DC current, weld time, and the distance between the tungsten electrode and gas cup (H), see Fig 2(b). The argon gas flow rate that is used throughout the whole welding process is constant (15 cubic feet per hour, cfh). The Samples are welded using the conditions as shown in Table 2.

Mechanical testing

Tensile-shear tests of 304 stainless steel joints were conducted on a universal testing machine (type WEW-100) with a maximum load of 100 kN. The tensile shear specimen for weld joints has dimensions of 25 mm wide, 175 mm long, and a 25 mm overlap, according to the American Welding Society (AWS) B.4 standard (see Fig 1). The crosshead velocity of the tensile shear test was 2 mm/min. The hardness of the weld joint cross-section was determined by Vickers microhardness testing with a load of 0.458 kg for a loading time of 15 s. The toughness of the welding joints, or the energy absorbed to failure, was determined from load-displacement curves using OriginPro® 2018. Nugget size was calculated using ImageJ.

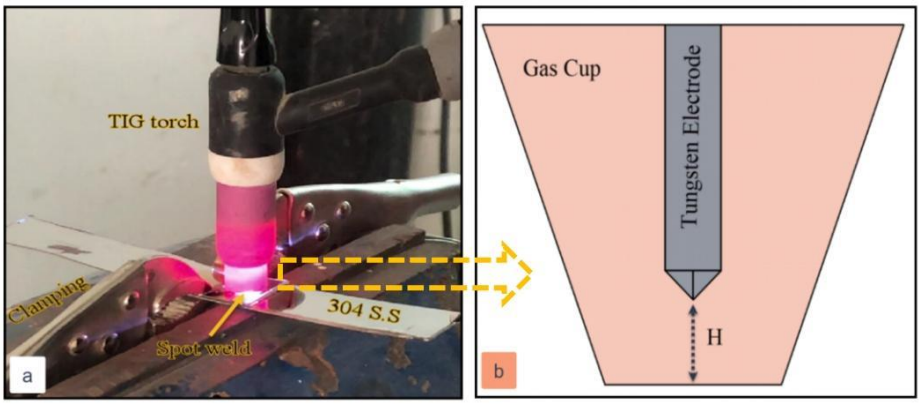

Fig. 2. (a) A schematic illustration of the fixture method of samples and (b) the distance between the tungsten electrode and the gas cup (H).

Table 2. TIG welding parameters used in this research

Experiment number	DC current (A)	Weld time (Sec)	H (mm)
A1	45	3	1.5
A2	45	5	1.5
A3	45	3	3.0
A4	45	5	3.0
A5	60	3	1.5
A6	60	5	1.5
A7	60	3	3.0
A8	60	5	3.0
A9	75	3	1.5
A10	75	5	1.5
A11	75	3	3.0
A12	75	5	3.0
A13	90	3	1.5

https://doi.org/10.24191/jmeche.v23i1.8443

RESULTS AND DISCUSSION

Microstructure characterization

When examining the weld sample, the following areas were observed: FZ (fusion zone), PMZ (partially melted zone), HAZ (heat-affected zone), and BM (base metal). It was found that the microstructure of BM-AISI 304 consists of an austenite phase, and the presence of twins was also observed, as shown in Fig 3. It was also noted that the FZ region of all the welded specimens contains a delta ferrite phase (δ) immersed in an austenite matrix(γ). It was noticed that the light area explains the (δ) ferrite phase, while the dark area represents the (γ) austenite phase. The δ phase enhances weld tensile strength, depending on its quantity (Hassan et al., 2023). The weld zone microstructure at low heat input consists of fine austenite grains due to the high cooling rate, which prevents granular growth. In addition to the existence of an amount of delta ferrite, which may be lower compared to the welding zone at high heat input (Randhawa & Kumar, 2018).

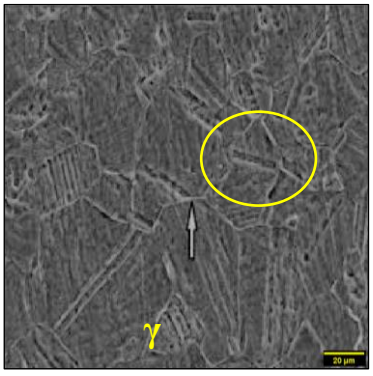

Fig. 3. AISI 304 stainless steel BM microstructure.

It was also noted that the microstructure, when the input temperature was increased, became rougher than at medium and low temperatures, due to the low cooling rate, which allows granular growth and the transformation of delta ferrite into austenite. The δ-ferrite amount that forms in the welding zone (FZ) is dependent on the heating input because the low cooling rate allows the δ-ferrite to transition into austenite over time, which results in a decrease in the amount of ferrite phase as the heat input level increases, as shown in Fig 4.

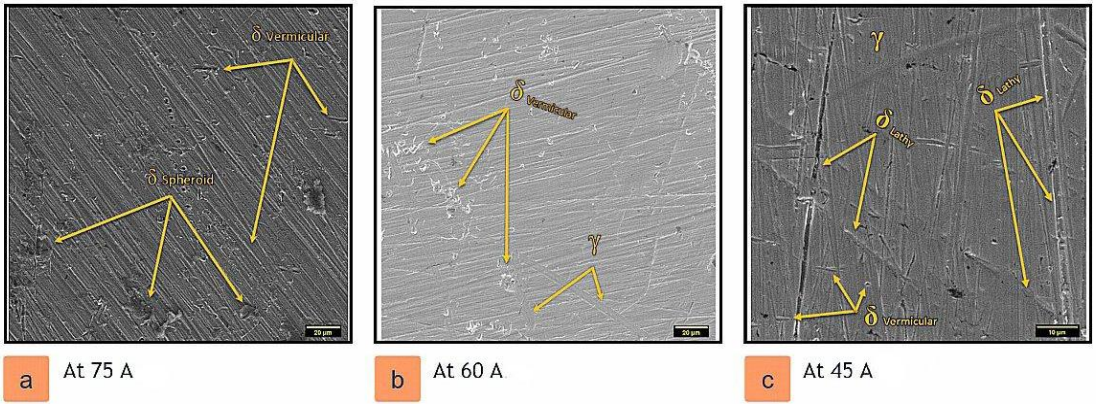

Fig. 4. SEM of weld metal samples (a) FZ-A9, (b) FZ-A6, and (c) FZ-A2.

https://doi.org/10.24191/jmeche.v23i1.8443

The existence of globular δ-ferrite was also observed in sample number A9, which improved the mechanical features (Arh et al., 2021). Additionally, it was demonstrated that lathy δ-ferrite appeared with vermicular δ-ferrite as a result of the reduction in heat input (Kumar & Shahi, 2011; Ogundimu et al., 2019), as demonstrated in Fig 4. Additionally, it was detected that sample number A9's vermicular ferrite is more discontinuous than that of the medium and the lowest level of heat input.

Tensile shear strength

The tensile test results (Table 3) show that the minimum tensile strength of 289 N was obtained with specimen number A3, representing the lowest heat input condition. This poor performance was caused by shorter welding time (t) and a larger electrode-to-gas cup distance (H), which reduced power density, resulting in insufficient heat accumulation, shallow weld penetration, and a small nugget diameter . However, an increase in welding current with a fixie (t and H) resulted in a dramatic enhancement of tensile strength owing to increased heat input to the FZ. For instance, tensile force increased from 803 N in specimen number A1 to 3822 N in specimen number A6 as the current was raised from 45 A to 60 A. This strength enhancement can be explained by the relatively lower quenching rate, which allowed more time for δ-ferrite to transform to γ-austenite, further improving the load-carrying capacity of the weld (Chuaiphan & Srijaroenpramong, 2020).

Table 3. Tensile features of the BM and weld metals

Experiment number	T.S. force (N)	Average nugget diameter (mm)	Weld toughness (J)
A1	803	3.11	0.236
A2	1465	3.62	0.055
A3	289	2.13	0.354
A4	684	2.53	0.082
A5	2583	4.76	1.983
A6	3822	5.18	4.629
A7	2121	4.60	0.931
A8	3234	5.01	4.027
A9	4179	5.65	5.529
A10	3906	5.39	5.526
A11	3444	5.11	3.663

The simultaneous effect of duration of welding and perpendicular distance between electrodes on heat input, therefore also the mechanical behavior, is further elucidated in Fig 5. The tensile strength of the sample A9 (welded with 75 A under optimized parameters) is at the maximum magnitude of 4179 N due to the optimal amount of δ-ferrite for ductility and toughness. On the other hand, specimen number A10 exhibited lower tensile strength, even at the same current level, because δ-ferrite content was lower and the weld structure became brittle (Bansod & Patil, 2017; Kumar & Shahi, 2011). At the maximum current level of 90 A (sample number A13), tensile strength decreased due to the overheating effect, resulting in over-penetration and local reduction of the weld specimen, as shown in Fig 6. Fractographic analysis also indicated that in all specimens, the partially melted zone (PMZ) near the fusion line (FL) was found to be the critical area controlling tensile failure in TIG spot-welded AISI 304 stainless steel joints.

Toughness of weld joints

Fig 7 shows the variation in weld toughness with respect to these welding parameters. A strong relationship between welding current and weld toughness was observed, with weld toughness improving with each increment of welding current, as the higher heating input affects the FZ microstructure. The highest impact toughness magnitude, 5.529 J, appears in sample number A9, which has the best ratio of δ-ferrite and γ-austenite phases. In the state, a low-hardness delta–ferrite phase with a hardness lower than

https://doi.org/10.24191/jmeche.v23i1.8443

that of the γ-phase had an optimum time to partially transform into austenite during cooling, thereby improving formability and energy absorption. On the contrary, the specimen number A10 had relatively lower toughness with increasing electrode-to-gas cup spacing (*H*), which decreased arc concentration and heat input in the weld area. This reduced local thermal input hindered the transformation to *δ*-ferrite, thereby reducing toughness. The worst results were obtained for the specimen with number A13, in which an excessive heat input had produced overpenetration and local lack of material at the weld, where both strengths and toughness were reduced. These results highlight the importance of the controlled heat input in achieving a balance between metallurgical and mechanical performance of TIG spot welds made in austenitic steels.

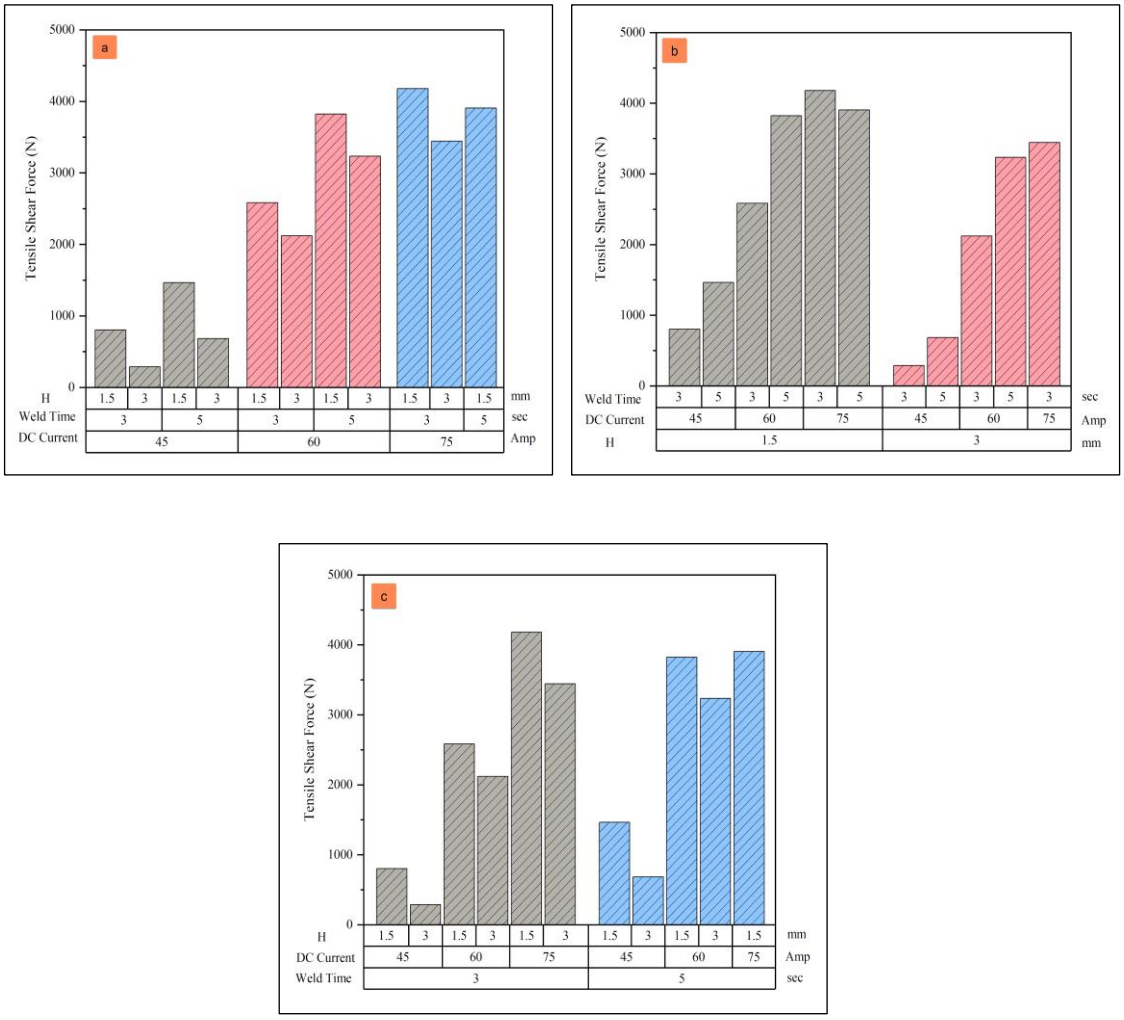

Fig. 5. Tensile shear force with (a) DC current, (b) the distance between the tungsten electrode and the gas cup (*H*), and (c) weld time.

https://doi.org/10.24191/jmeche.v23i1.8443

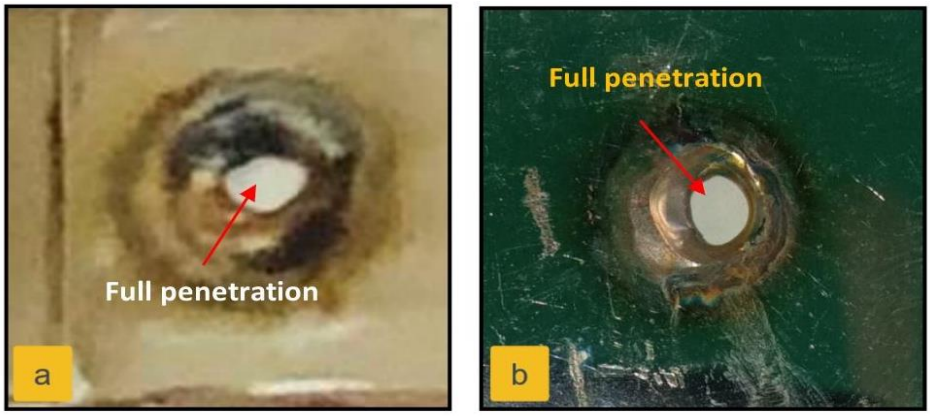

Fig. 6. Full penetration of joints at: (a) 75 A, 5 s and (b) 90 A, 3 s.

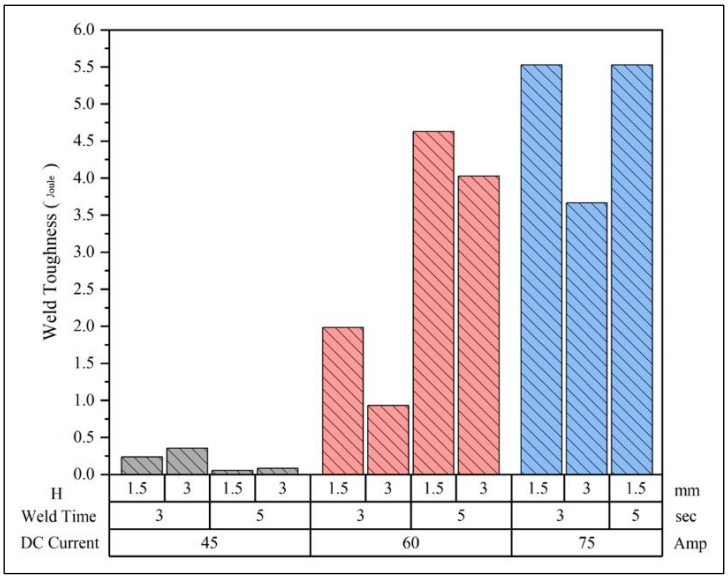

Fig. 7. Weld toughness with different welding parameters.

Nugget size

The average weld-nugget diameter was found to strongly influence the applied welding parameters, as shown in Fig 8. Changes in heat input, controlled by the electrode-to-cup distance (*H*), duration, and welding current, directly affected nugget shape. Nugget height decreased, and average nucleation diameter increased as a function of increasing current from 45 A to 60 A, then 75 A, suggesting that more thermal energy is being delivered to the weld region (Charde, 2012). Among all specimens, the number A9 sample produced under 75 A, intermediate dwell time, and reduced (*H*) demonstrated the largest nugget diameter, as illustrated in Fig 9. Conversely, nugget size was diminished when (*H*) was increased, when welding current was lowered, or when dwell time was shortened. The combined effect of high current, extended welding time, and reduced (*H*) substantially elevated heat input, promoting increased molten metal volume and lateral spread of FZ. However, excessive heat input was found to induce over-penetration and local thinning of the weld region, which may adversely affect structural integrity in service.

https://doi.org/10.24191/jmeche.v23i1.8443

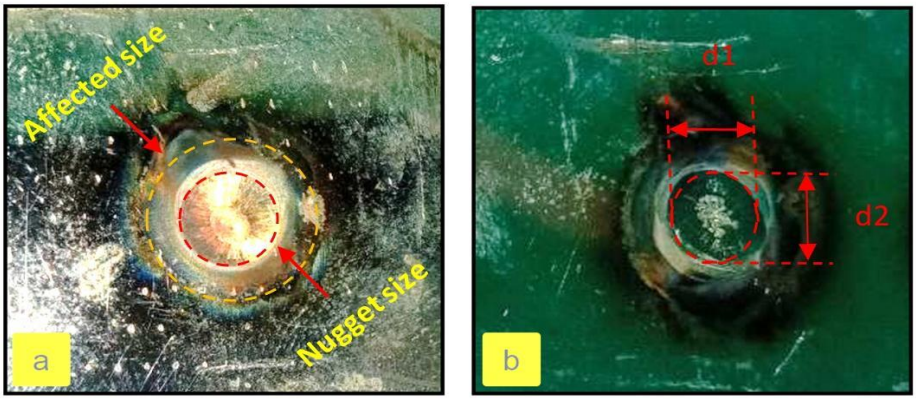

Fig. 8. (a) Affected and nugget size and (b) the diameters of the nugget size.

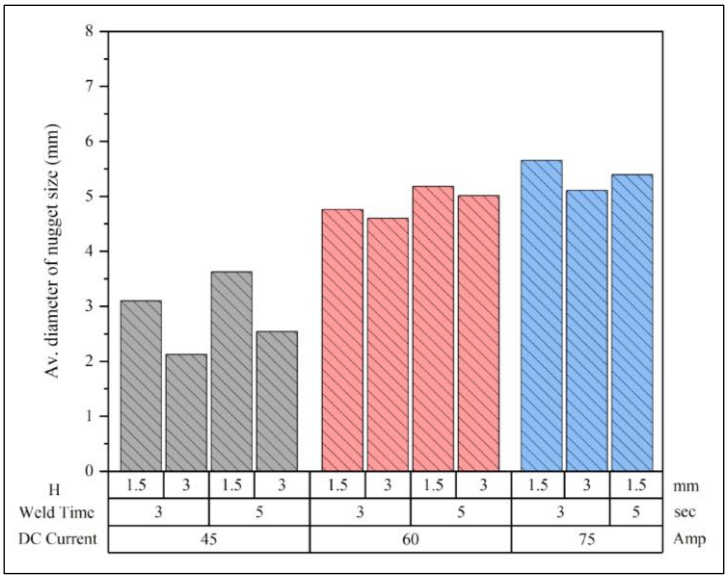

Fig. 9. Average nugget size of all the parameters.

Microhardness of weld joints

Fig 10(a) and Fig 10(b) present the microhardness distribution across the weld cross-section for representative high-, medium-, and low-heat-input conditions. Indentations were spaced at 0.5 mm intervals from FZ through the PMZ, HAZ, and into BM on both sides of the weld line. At high heating input, the FZ exhibited reduced hardness compared with the medium- and low-heat-input specimens, a trend attributed to increased δ-ferrite formation due to slower cooling rates and extended solidification times. Medium heat input (specimen number A6) produced the maximum FZ hardness of 250 HV, while high heat input (specimen number A9, 75 A) reduced FZ hardness to 225 HV due to δ-ferrite coarsening and $\gamma \rightarrow \delta$ transformation. Low heat input (specimen number A2) yielded 232 HV, reflecting finer dendritic microstructures (M. Jebbur et al., 2022).

https://doi.org/10.24191/jmeche.v23i1.8443

In all the specimens, the hardness was higher in the PMZ compared with that of FZ because $Cr_{23}C_6$ carbides and residual austenite, as well as some (unresolved) δ-ferrite having relatively higher hardness than δ-ferrite-dominated FZ, were present. The HAZ, including the PMZ, had lower hardness in the CGHAZ, which increased toward BM, where FG structures were more prevalent. The variations in these gradients are consistent with a local thermal history, e.g., slower cooling in the vicinity of PMZ favors δ-ferrite formation and carbide precipitation, while faster cooling at BM refines grain size and enhances its hardness. The observed profiles are consistent with earlier findings on the relationship between heat input and δ-ferrite morphology, carbide precipitation, and microhardness variation in GTAW of austenitic stainless steels (Chuaiphan & Srijaroenpramong, 2014, 2020; Alkhafaji et al., 2025).

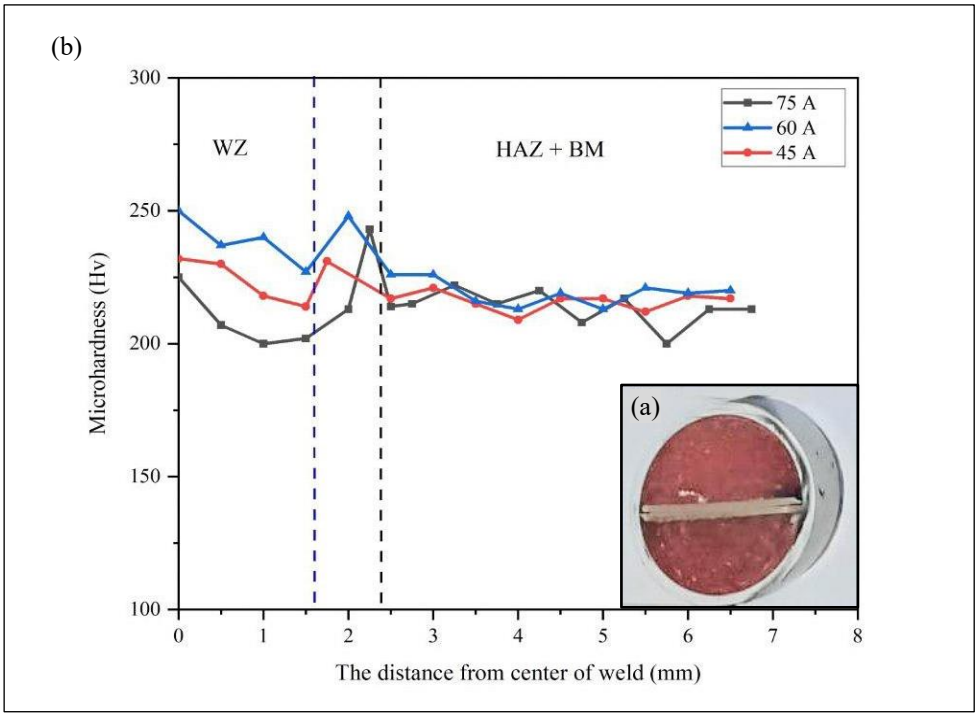

Fig. 10. (a) The weld joint cross-section and (b) the microhardness distribution of AISI 304 weld joints.

CONCLUSION

This experimental investigation established a clear relationship between TIG spot-welding parameters, heat input, and the resulting microstructural evolution and mechanical performance of AISI 304 austenitic stainless-steel joints within the investigated current range of 45 A to 90 A, welding durations up to 3 s, and sheet thicknesses of 1.5 mm to 3.0 mm. The fusion zones were characterized by δ-ferrite dispersion within an austenitic matrix, with ferrite morphology transitioning from predominantly lathy at low heat inputs to vermicular and globular forms as thermal energy increased. An intermediate heat input condition (75 A, 3 s, 1.5 mm) yielded the most favorable combination of tensile shear strength (4179 N), impact toughness (5.529 J), and nugget diameter (5.65 mm), attributed to an optimized δ-ferrite fraction and refined microstructural features. Conversely, excessive heat input at 90 A resulted in over-penetration, pronounced grain coarsening, and deterioration of both mechanical strength and hardness, emphasizing the necessity of avoiding high-energy regimes in thin-gauge stainless steels. The maximum microhardness value (250 HV)

https://doi.org/10.24191/jmeche.v23i1.8443

was achieved under moderate heat input, while further energy input promoted δ-ferrite coarsening and corresponding hardness reduction within the fusion zone. Fracture consistently initiated within the partially melted zone, highlighting its critical influence on joint integrity and the need for stringent process control to minimize metallurgical discontinuities in this region. Collectively, the findings delineate an optimal welding window for producing high-strength, high-toughness TIG spot welds in AISI 304 stainless steel, with future investigations recommended to explore the influence of filler material addition on microstructural refinement and joint performance.

ACKNOWLEDGEMENT

The authors would like to thank the Ministry of Higher Education, University of Kufa, and Imam Ja'afar Al-Sadiq University. This work was conducted in the laboratory at the University of Kufa.

FUNDING

No external funding.

CONFLICT OF INTEREST

The authors declare that no conflict of interest.

AUTHORS' CONTRIBUTION

Mohammed K. Aljanabi conceived the research idea, designed the experimental methodology, and conducted experimental work. Marwah Mohammed Abdulridha and Ekhlas Hassan carried out the tests results analysis. Zainab Al-Khafaji performed manuscript preparation and critical revision of the final manuscript..

REFERENCE

Aliyari, H., Miresmaeili, R., & Azadi, M. (2025). Fatigue life prediction of spot-welded joints using a novel indentation technique for precise elastoplastic characterization of weld zones. Journal of Materials Research and Technology, 35, 2087–2102. https://doi.org/10.1016/j.jmrt.2025.01.116

Arh, B., Tehovnik, F., & Vode, F. (2021). Transformation of the δ-Ferrite in SS2343 austenitic stainless steel upon annealing at 1050 °C, 1150 °C and 1250 °C. Metals, 11(6), 935. https://doi.org/10.3390/met11060935

Banerjee, P., Sarkar, R., Pal, T. K., & Shome, M. (2016). Effect of nugget size and notch geometry on the high cycle fatigue performance of resistance spot welded DP590 steel sheets. Journal of Materials Processing Technology, 238, 226–243. https://doi.org/10.1016/j.jmatprotec.2016.07.023

Bansod, A. V., & Patil, A. P. (2017). Effect of welding processes on microstructure, mechanical properties,

and corrosion behavior of low-nickel austenitic stainless steels. Metallography, Microstructure, and Analysis, 6(4), 304–314. https://doi.org/10.1007/s13632-017-0368-3

Cai, H., Xu, L., Zhao, L., Han, Y., & Guo, X. (2023). Microstructure and mechanical properties of 9Cr-3Co-2.9 W-CuNbV steel welded joints processed by different tungsten inert gas (TIG) welding. Materials Characterization, 199, 112840. https://doi.org/10.1016/j.matchar.2023.112840

Casanueva, R., Brañas, C., Diaz, F. J., Azcondo, F. J., Ferreño, D., & Setien, J. (2023). Characterization of an energy efficient pulsed current TIG welding process on AISI 316 and 304 stainless steels. Heliyon, 9(9), e19819. https://doi.org/10.1016/j.heliyon.2023.e19819

Charde, N. (2012). Spot weld growth on 304L austenitic stainless steel for equal and unequal thicknesses. Caspian Journal of Applied Sciences Research, 1(11), 83-91.

Chen, Y., Zhao, X., Yang, B., Liu, Y., Liang, Y., Li, Z., & Chen, C. (2024). Study on properties of 304 wire arc additive manufacturing stainless steel TIG welded joints. Materials Letters, 361, 136107. https://doi.org/10.1016/j.matlet.2024.136107

Chuaiphan, W., & Srijaroenpramong, L. (2014). Effect of welding speed on microstructures, mechanical properties and corrosion behavior of GTA-welded AISI 201 stainless steel sheets. Journal of Materials Processing Technology, 214(2), 402–408. https://doi.org/10.1016/j.jmatprotec.2013.09.025

Chuaiphan, W., & Srijaroenpramong, L. (2020). Microstructure, mechanical properties and pitting corrosion of TIG weld joints alternative low-cost austenitic stainless steel grade 216. Journal of Advanced Joining Processes, 2, 100027. https://doi.org/10.1016/j.jajp.2020.100027

Groover, M. P. (2012). Fundamentals of modern manufacturing: materials, processes, and systems. (5th Ed.). Wiley Global Education.

Hassan, A., El-Mahallawi, I. E., & El-Koussy, M. R. (2023). Effect of GTAW welding current on the quality of 304L Austenitic Stainless steel using ER316L. International Journal of Materials Technology and Innovation, 3(2), 10–18. https://doi.org/10.21608/ijmti.2023.190981.1075

Hayat, A.A., Aminy, A.Y., 2022. The Effect of Spot Welding Parameters for Dissimilar Material Mild Steel and Galvanizes Steel on Nugget Size and Mechanical Strength. EPI International Journal of Engineering, 5, 104–109. https://doi.org/10.25042/epi-ije.082022.05

Kishore, K., Kumar, P., & Mukhopadhyay, G. (2019). Resistance spot weldability of galvannealed and bare DP600 steel. Journal of Materials Processing Technology, 271, 237–248. https://doi.org/10.1016/j.jmatprotec.2019.04.005

Kumar, S., & Shahi, A. S. (2011). Effect of heat input on the microstructure and mechanical properties of gas tungsten arc welded AISI 304 stainless steel joints. Materials & Design, 32(6), 3617–3623. https://doi.org/10.1016/j.matdes.2011.02.017

M. Alkhafaji, M., K. Aljanabi, M., & Dakhel Fahad, N. (2025). Investigation of re-spot effects on mechanical properties in resistance spot welding of low carbon steel. Journal of Advanced Research in Applied Mechanics, 136(1), 153–164. https://doi.org/10.37934/aram.136.1.153164

M. Jebbur, A., Abed AlKareem, S. S., & Mustafa, F. F. (2022). Effect of MIG welding parameters on the mechanical properties of AISI 304 austenitic stainless steels. Al-Khwarizmi Engineering Journal, 18(1), 1–15. https://doi.org/10.22153/kej.2022.01.001

Muñoz, J. A., Komissarov, A., Mejía, I., Hernández-Belmontes, H., & Cabrera, J. M. (2021). Characterization of the gas tungsten arc welding (GTAW) joint of Armco iron nanostructured by equal-

https://doi.org/10.24191/jmeche.v23i1.8443

channel angular pressing (ECAP). Journal of Materials Processing Technology, 288, 116902. https://doi.org/10.1016/j.jmatprotec.2020.116902

Ogundimu, E. O., Akinlabi, E. T., & Erinosho, M. F. (2019). Effect of welding current on mechanical properties and microstructure of TIG welding of type-304 austenite stainless steel. Journal of Physics: Conference Series, 1378(3), 32022. https://doi.org/10.1088/1742-6596/1378/3/032022

Pasupulla, A. P., Agisho, H. A., Seetharaman, S., & Vijayakumar, S. (2022). Characterization and analysis of TIG welded stainless steel 304 alloy plates using radiography and destructive testing techniques. Materials Today: Proceedings, 51(1), 935–938. https://doi.org/10.1016/j.matpr.2021.06.305

Radhi, N. S., & Al-Khafaji, Z. (2018). Investigation biomedical corrosion of implant alloys in physiological environment. International Journal of Mechanical and Production Engineering Research and Development, 8(4), 247-256. https://doi.org/10.24247/ijmperdaug201827

Radhi, N. S., Al-Khafaji, Z., Mareai, B. M., Radhi, S., & Alsaegh, A. M. (2023). Reducing oil pipes corrosion by (Zn-Ni) alloy coating on low carbon steel substrate by sustainable process. Journal of Engineering Science and Technology, 18(3), 1624–1638.

Rajak, B., Kishore, K., & Mishra, V. (2023). Investigation of a novel TIG-spot welding vis-à-vis resistance spot welding of dual-phase 590 (DP 590) steel: processing-microstructure-mechanical properties correlation. Materials Chemistry and Physics, 296, 127254. https://doi.org/10.1016/j.matchemphys.2022.127254

Randhawa, H. S., & Kumar, S. (2018). Study of microstructure 304L austenitic stainless steel weld deposited by GTAW for root pass and SMAW for filler passes. Asian Journal of Engineering and Applied Technology, 7(2), 21–25. https://doi.org/10.51983/ajeat-2018.7.2.1010

Sabzi, M., Anijdan, S. H. M., Eivani, A. R., Park, N., & Jafarian, H. R. (2021). The effect of pulse current changes in PCGTAW on microstructural evolution, drastic improvement in mechanical properties, and fracture mode of dissimilar welded joint of AISI 316L-AISI 310S stainless steels. Materials Science and Engineering: A, 823, 141700. https://doi.org/10.1016/j.msea.2021.141700

Singh, R. P., & Agrawal, M. K. (2021). Effect of welding current on the dimensions of bead in tungsten inert gas welding process. Materials Today: Proceedings, 45(2), 3235–3239. https://doi.org/10.1016/j.matpr.2020.12.382

Tabrizi, T. R., Sabzi, M., Anijdan, S. H. M., Eivani, A. R., Park, N., & Jafarian, H. R. (2021). Comparing the effect of continuous and pulsed current in the GTAW process of AISI 316L stainless steel welded joint: microstructural evolution, phase equilibrium, mechanical properties and fracture mode. Journal of Materials Research and Technology, 15, 199–212. https://doi.org/10.1016/j.jmrt.2021.07.154

https://doi.org/10.24191/jmeche.v23i1.8443